

**Characterizing the Effects of Asteroid Belt Perturbations on
the Orbits of the Inner Planets**

**New Mexico
Supercomputing Challenge
Final Report
April 07, 2011**

**Team #7
Albuquerque Academy**

**Team Member: Nikita Bogdanov
Teacher: Mr. Jim Mims
Mentor: Dr. Marc A. Murison**

□

Executive Summary:

The planets in the solar system are subject to multiple gravitational perturbations from other solar system bodies including those from general relativity, solar oblateness, other planets, large asteroids (as discrete point masses), and small asteroids (cumulatively). The largest uncertainty in our knowledge of the orbits of the inner planets, Mercury, Venus, Earth, and Mars, is due to perturbations from the complicated and uneven mass distribution within the asteroid belt.

The goals of this project are to analyze this distribution and to computationally model the effects of its perturbations on the orbits of the inner planets; specifically, this project looks to characterize the perturbative effects as a noise problem. In order to do this, we have created first a flexible, object-oriented framework in Python for the integration of dynamical systems. This generalized ODE solver was then adapted to address several questions regarding planetary motions as subject to asteroid belt perturbations.

Table of Contents:

1	Introduction
1.1	Previous Work
1.2	This Project
2.	Computational Model
2.1	Framework Development Using a Test Problem
2.2	The Solar System Problem
2.3	Numerical Techniques
3	Results
4	Conclusions
5	Future Work

Works Cited

Appendix A Figures

1 Introduction:

The planets of the solar system are subject to various gravitational perturbations from other bodies. These perturbations include the other planets, large asteroids (as discrete point masses), small asteroids (cumulatively), solar oblateness, and those caused by relativistic effects.

Although spacecraft range and range-rate observations have led to the development of high accuracy ephemerides, especially for the inner solar system planets (Newhall et al. 1983) there are still uncertainties of up to 1km (Standish and Fienga 2002) in inner solar system planetary positions. Currently, the largest uncertainty is believed to be due to the asteroids (Standish and Fienga 2002). As of this writing, there are approximately 541,000 known asteroids (Bowell 2010) in the main asteroid belt, unevenly distributed between the orbits of Mars and Jupiter.

A large range in the masses of the objects further complicates this uneven distribution. Most of the mass of the asteroid belt is contained within four bodies, meaning that almost all other individual asteroids perturb the planets by small to negligible amounts. However, the collective influence of small asteroids on the orbits of the planets is significant to some extent, which has yet to be investigated in future research. The accuracy of current orbital predictions is limited largely because of these perturbations from the asteroid belt. This presents the challenge of how to accurately navigate the solar system, without an accurate knowledge of the orbits.

1.1 Previous Work:

There have been several studies that have analyzed the effects of asteroid belt perturbations; these have focused primarily on the refinement of high-precision ephemerides, on the increase of the accuracy of asteroid models, and on the determination of the most significant perturbers and their effects, among other things.

Notably, Fienga and Simon (2005) consider the perturbative effects of 300 asteroids on the orbits of the inner planets. Their primary motivations were to develop in parallel an improved analytical model and an accurate numerical integration for the inner solar system. To come to their conclusions, they use two separate approaches in their study, analytical, and direct

numerical integration, and compare their accuracy to that found in the JPL ephemerides. They find that:

- Asteroid perturbations on Mercury and Venus are non-negligible.
- The accuracy of their analytical model is comparable to that of high-precision numerical integrations.
- Inner asteroid (Apollo-Aten-Amor) perturbations are “quite-negligible” for short-term inner solar system dynamics. □ □

Later, Kuchynka et al. (2010) assess the ability of a ring model of the small mass asteroids to successfully model perturbations from the main asteroid belt. They estimate the asteroid perturbations by comparing results from integrations including and excluding the ring; in order to evaluate the ring’s capacity to model many individual objects, they compare it against many test models, each containing a different set of individual asteroid masses. Such Monte-Carlo experiments can provide estimates as to how many asteroids need to be individually modeled in order to maintain accurate results. □

1.2 This Project:

Thus, the focus of this project is to characterize the perturbative effect of the asteroids on the motions of the inner planets rather than to further refine ephemerides; specifically, this project looks to characterize the perturbative effects as a noise problem, which is a novel and promising approach. However, at the current stage of research, only qualitative data is presented; this data is the first step though to noise characterizations. □ □

2 Computational Model:

The computational model that we implement has a complex structure, which, without a starting framework to build off of, would be very difficult to create and debug from scratch. The framework must be flexible and object-oriented in order to be easily adaptable in the future. As well, it must properly integrate the equations of motion to give accurate results; we will thus have to prove that it is behaving correctly. Throughout the research, this framework has evolved significantly and is in fact completely different from the initial design.

2.1 Framework Development Using a Test Problem:

We created first a program that integrates the equations of motions to find the trajectory of an earth bound projectile in the presence of air resistance and a steady wind from an arbitrary direction. This is a very simple physics problem (Figure 1), and without air resistance, can be solved analytically, allowing confirmation that the integrating machinery is working properly. The user can set the initial environmental conditions, launch conditions, and modeling conditions, to achieve different types of trajectories. This allows the model to more realistically approximate what we actually observe.

A useful experiment that I preformed was to determine the effect of step-size on ODE integration accuracy. I observed errors due both to very small and to very large step-sizes. At very small step-sizes, the accuracy fluctuates in the range, which appears to be the numerical round-off noise floor. Above a certain threshold, the accuracy degrades exponentially until a step- size of significant magnitude causes fluctuations in the accuracy at the upper end as well (figure 2). This pattern of an exponential increase in error as a function of step-size, with upper and lower bounds is what is expected. □□□□

The error at large step-sizes is due to series expansions inherent in the numerical integration algorithm being truncated at each iteration, leading to an accumulation of error by the end of the integration. For very small step-sizes, I saw round off error present in the end conditions. This error was caused by the limited number of floating point decimals available on my machine, and the inability to produce values with infinite precision each step. However, having a machine with infinite precision, we would still suffer from truncation error. Numerical issues such as this must be kept in mind for any dynamical computation. Being able to implement an ODE solver, and understand how it works, requires knowing the mathematical concepts behind the problem at hand. Thus, in order to create the ODE solver framework, I have been learning about vectors and vector algebra; differentiation, series expansions, and integral calculus; particle dynamics in two and three dimensions; ODEs and numerical techniques for solving ODEs. □□

To control such numerical errors from entering the integration, the solar system framework makes use of an adaptive step size integration method, which can control for error terms. □□

2.2 The Solar System Problem □ □

All of the data used in this project is either calculated or obtained from a database. Specifically, planet orbital elements are calculated within the framework for a specific date. All asteroid data however is obtained from the Bowell asteroid database, which contains over 541, 000 objects. The ten asteroids that are integrated in this project are the ten largest asteroids in the asteroid belt: Ceres, Pallas, Juno, Vesta, Astraea, Hebe, Iris, Flora, Metis, Hygiea. Whenever only one asteroid is integrated it is always Ceres. □ □

In this study, we implement a high-precision, short-timescale ($10^2 - 10^4$ years) numerical integration of the planets and asteroids, and in the future will determine the applicability and dynamical importance of various methods of approximating the main-belt asteroid mass distribution. Although this implementation is based on the generalized framework presented in 2.1, it has been vastly modified and improved from its original state. □

The equations of motion for the solar system model, with the coordinate origin coincident with the sun, and addressing only the point masses within the asteroid belt, are: □ □

$$\frac{d^2 \vec{r}_k}{dt^2} + G(m_0 + m_k) \frac{\vec{r}_k}{|\vec{r}_k|^3} = G \sum_{\substack{i=1 \\ i \neq k}}^N m_i \left(\frac{\vec{r}_i - \vec{r}_k}{|\vec{r}_i - \vec{r}_k|^3} - \frac{\vec{r}_i}{|\vec{r}_i|^3} \right)$$

where N is the number of discrete masses other than the sun, m_0 is the mass of the sun, and m_k and m_i are the masses of bodies k and i , respectively. To make this equation unit less, we put m in solar masses, r in Astronomical Units, and t in Earth periods. This not only simplifies the equation, but also improves the robustness of numerical computations; now we model with solar masses, Astronomical Units, and Earth years (instead of kilograms, meters, and seconds.) Doing this, we obtain, for the k^{th} body: □ □ □ □

$$\frac{d^2\vec{r}_k}{dt^2} + \frac{1 + \mu_k}{1 + \mu_E} \frac{\vec{r}_k}{|\vec{r}_k|^3} = \sum_{\substack{i=1 \\ i \neq k}}^N \frac{\mu_i}{1 + \mu_E} \left(\frac{\vec{r}_i - \vec{r}_k}{|\vec{r}_i - \vec{r}_k|^3} - \frac{\vec{r}_i}{|\vec{r}_i|^3} \right)$$

where μ_k and μ_i are the scaled masses of the k^{th} and i^{th} bodies, respectively, and $\mu_E = M_E / M_{Sun}$. Our knowledge of the value of G and, separately, of the masses of objects in the solar system is not very accurate. Fortunately, this issue is partly resolved due to the way in which we measure the masses of solar system objects. Because of the nature of Newton's equations, and specifically Kepler's third law,

$$P^2 = \frac{4\pi^2}{G(m_1 + m_2)} a^3$$

when we measure the period and the semi-major axis of mass m_1 interacting with mass $m_2 < m_1$, the resulting measurement is actually of the product Gm_1 and is more precise than our knowledge of G or m_1 separately. To obtain μ , we divide the mass of the object by the mass of the sun; because both of these values are measured in Gm , we retain the measurement precision of Gm in the values of μ . During the integration, the positions and velocities of all of the bodies in the model are stored in a large state vector array; the first half contains the x, y, and z positions, and the second half contains the x, y, and z velocities for all bodies in a consistent order. All information about the state of the model can be derived from this state vector and from the independent variable, time. □ □

The integration framework advances the system via an adaptive step-size 8th order Runge-Kutta method (Press et al. 2007). It has three interaction parameters that define how solar system objects interact with each other.

- 1 All – all bodies interact with other bodies.
- 2 Partial – all bodies interact with other bodies, except asteroids do not feel other asteroids

- 3 Restricted – all bodies interact with other bodies, except asteroids do not feel other asteroids and planets do not feel asteroids. This is known as the semi-restricted N body problem. □ □

In the final results calculations, all bodies interacted other bodies. However, by looking at the residuals of identical all and partial runs, it was determined that there is no significant difference between the two. In fact, figure 3 shows a residual plot for partial vs. all runs, and it is seen that the difference is only very small, but also advances in a way indicative of numerical noise.

Initially, baseline integrations of planets with and without perturbers were performed in order to qualitatively analyze the behavior of planets under varying circumstances. These test included both asteroid and planetary perturbers. The results from these can be seen in figures 4-6. Figure 7 shows the residuals for a 10, 000 year integration of the 8 planets and 10 largest asteroids.

- 1 The analysis of asteroid perturbations on planetary motion employed two analysis techniques. Examine the residuals of chosen orbital elements of two separate integrations, differing only in that one included perturbing asteroids while the other did not. The residuals provided an idea of the scale of the perturbations. The residuals in the semi-major axis of Earth and Mars were noted to be in the 1×10^{-8} AU region. □ □
- 2 Power spectra for the residuals of no asteroid-asteroid integrations were calculated. These are the first step in characterizing gravitational perturbations as a noise problem. Furthermore, they can reveal planet-planet and planet-asteroid resonances. □ □

During the course of this research, it was also assumed that an absolute error tolerance of 1×10^{-7} was sufficient and at the level of the uncertainties in initial conditions. This was later verified by running two identical integrations, differing only in the absolute tolerance parameter, and looking at the residuals from one orbital element. The characteristic expansion of the residuals as a function of t^2 and a comparatively small difference between Absolute Tolerance = 10^{-8} and 10^{-7} vs. Absolute Tolerance = 10^{-6} and 10^{-8} confirmed that the differences were due to numerical noise and that Absolute Tolerance = 10^{-7} was sufficient. Plots comparing absolute tolerances can be seen in figures 8 and 9.

2.3 Numerical Techniques

The internal optimization of our program consists of removing all unnecessary calculations of square roots, which is used in order to calculate distances between objects, as well as making use of specialized Python libraries (numpy, cython) for numerically intensive sections of code. Thus, we retain the functionality and ease of use of Python, an interpreted language, while achieving numerical speeds comparable to those of compiled languages. In order to calculate the accelerations on an object from the other bodies, we use nested for loops. In the calculation of this acceleration, the distances between bodies are actually used twice per pair; once from object k to i , and once from i to k . Thus, we simply calculate the distances to and from all bodies once, up front, and then use these values within the body interaction for-loop. As well, we implement an 8th order adaptive step-size Runge-Kutta algorithm (Press et. al, 2007), which not only allows us to control error terms, but also increases integration speeds. □ □

3 Results □ □

The residual plots are the first step to characterizing perturbations as a noise problem; using these perturbation power spectra can be calculated using an FFT. This takes a signal in the time domain and re-expresses it in the frequency domain, showing at which frequencies the power of the signal is located. In an ideal situation, where we have an infinite signal, the Fourier Transform would produce delta function spikes at the peak power frequencies. However, in the real world we do not have infinite data sets and so the output of the Fourier Transform is in fact a sin cardinal function, which produces secondary lobes that radiate outwards from the central peak at any frequency. Interpreting whether what we see in our spectral plots is just noise or real effects is thus difficult. □ □

Because asteroid perturbations are all cyclical, each one operates at a certain frequency in the motion of any particular body. This shows up a cyclical variation of the orbital elements, and the power spectra reveal the density of perturbation frequencies. □ □

The magnitude of the perturbations is seen on the y-axis, and it demonstrates to what extent the planets, and more importantly planetary orbital elements, are jostled by each other and by the

asteroids, at peak frequencies. The power spectra are the first step to characterizing gravitational perturbations as a noise problem since we can contrast the power spectra of some of the standard noise types against what is seen in planetary motion to see similarities. □ □

The large spikes in the power spectra suggest that the gravitational perturbations caused by the inclusion of asteroids are largest at the frequencies at which one sees the spikes. That is to say that where a spike is observed, gravitational perturbations jostle the planet's given orbital element most at that frequency. □ □

Figures 10 and 11 show the power spectra for 10, 000 year integrations of the 8 planets and 10 asteroids or Ceres, respectively.

4 Conclusions

The so-far qualitative analysis of the power spectra for the gravitational perturbations caused by asteroids on the orbits of the inner planets show that there are certain frequencies at which a planet's orbital elements are perturbed at most. Having the power spectra for certain critical orbital elements, such as eccentricity and semi-major axis, is the first step to actually characterizing the perturbations as a noise problem, and to being able to calculate orbital probabilities for planets.

The most significant original achievement of the project is thus analyzing the power spectra of asteroid perturbations in an effort to classify them as noise.

5 Future Work □ □

Currently, asteroid gravitational perturbations are modeled by only the ten most massive asteroids. This is sufficient for gaining an understanding of the underlying characteristics of gravitational perturbations, but is not enough to begin accurate noise characterization. In order to more accurately model the interactions between the inner planets and the asteroids, I plan to simulate the latter using three distinct groups: the roughly half dozen largest asteroids which directly perturb the inner planets, the several hundred asteroids of smaller but still significant

mass, and the rest of the asteroids whose masses are individually not large enough to perturb the planets, but whose cumulative effects are not negligible.□□

There are also several interesting questions which come out of this initial research: □

- Fienga and Simon (2005) state that asteroid perturbations on Mercury and Venus are non-negligible. Are second order perturbations from these planets significant?□
- Which coordinate system is most advantageous, barycentric or heliocentric?□
- Can asteroid masses be extrapolated from the results and from measured planetary perturbations? If not, can bounds be placed on some masses?□
- Which components of the solar system model are most influential?
- At what level does chaos prevent the knowledge of planetary positions?
- Does the gravitational noise that we see look like any of the standard noise types?□□ These questions will be addressed in later research.□□□

Works Cited:

Bowell, E.: 2010, Lowell Observatory asteroid elements database.

URL: <ftp://ftp.lowell.edu/pub/elgb/astorb.html>

Fienga, A. and Simon, J.: 2005, Analytical and numerical studies of asteroid perturbations on solar system planet dynamics, *Astronomy and Astrophysics* 429(1), 361–367.

URL: <http://adsabs.harvard.edu/abs/2005A&A...429..361F>

<http://www.edpsciences.org/10.1051/0004-6361:20048159>

Kuchynka, P., Laskar, J., Fienga, A. and Manche, H.: 2010, A ring as a model of the main belt in planetary ephemerides, *Astronomy and Astrophysics* 514, A96.

URL: <http://adsabs.harvard.edu/abs/2010A%2526A...514A..96K>

<http://www.aanda.org/10.1051/0004-6361/200913346>

Newhall, X., Standish, E. and Williams JG: 1983, DE 102-A numerically integrated ephemeris of the moon and planets spanning forty-four centuries, *Astronomy and Astrophysics* 125, 150–167.

URL: <http://adsabs.harvard.edu/full/1983A&A...125..150N>

Press, W. H. et al. (2007). *Numerical Recipes: the Art of Scientific Computing*, Cambridge Univ. Press, 3rd ed.

Standish, E. M. and Fienga, A.: 2002, Accuracy limit of modern ephemerides imposed by the uncertainties in asteroid masses, *Astronomy and Astrophysics* 384(1), 322–328.

URL: <http://adsabs.harvard.edu/abs/2002A&A...384..322S>

<http://www.edpsciences.org/10.1051/0004-6361:20011821>

Special thanks to Dr. Marc A. Murison and the US Naval Observatory – Flagstaff Station

Appendix A: Figures

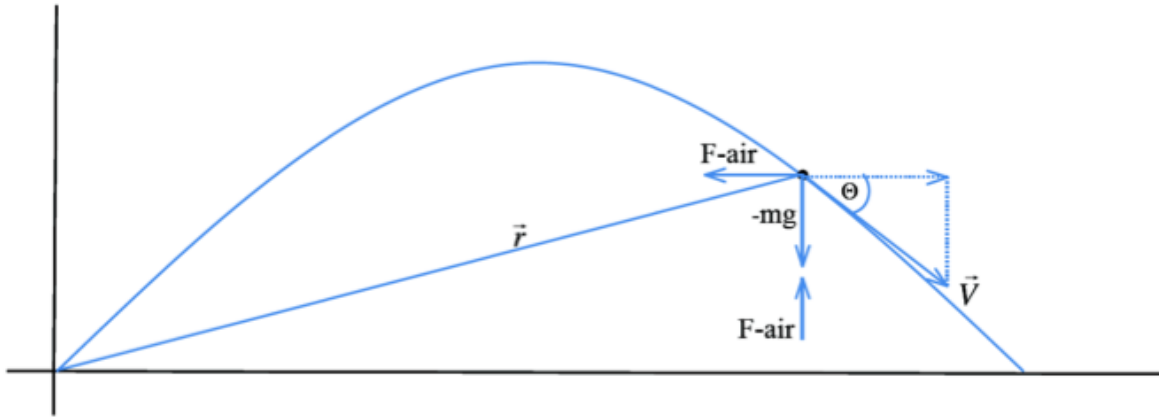


Figure 1: This figure diagrams the forces acting on an earth-bound projectile. Air resistance will almost always act against the x, y, and z components of velocity; additionally, gravity will always act on the projectile in the y direction.

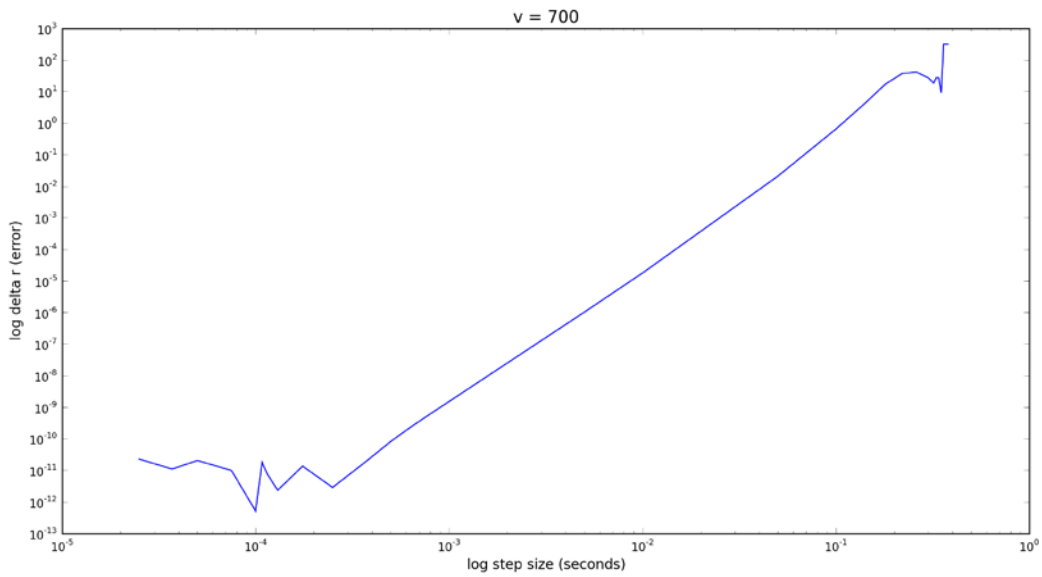


Figure 2: This plots shows the exponential decrease in accuracy with increasing integration step-size. (elevation=45deg, wind=0, m=0.5kg, c=0.005)

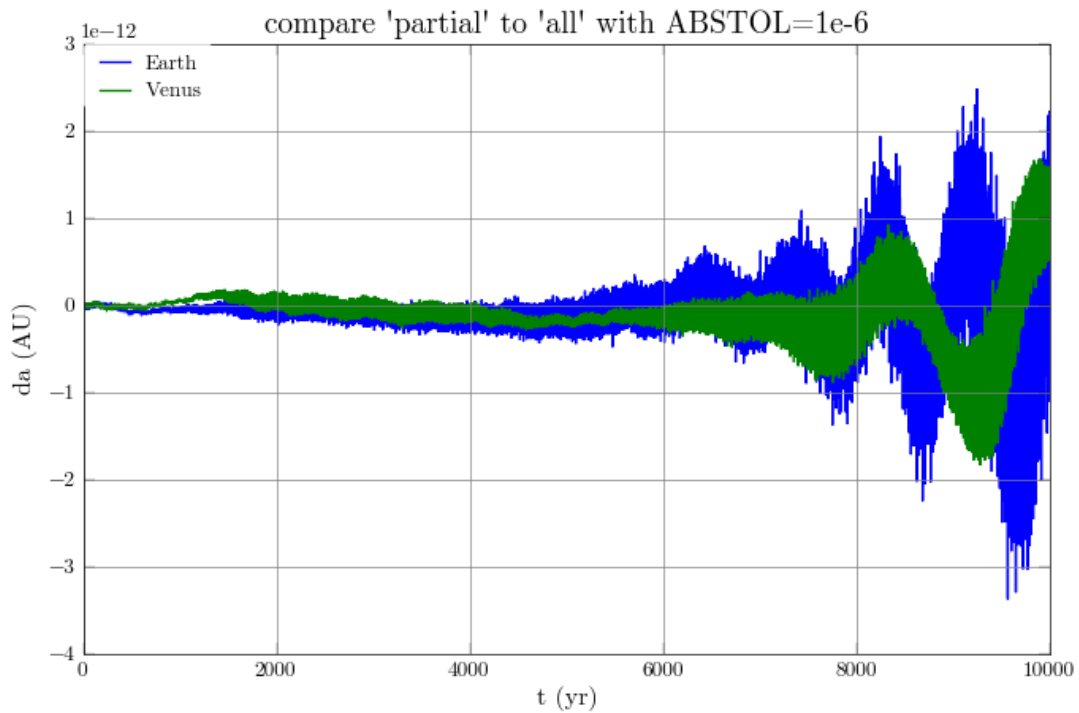


Figure 3: A partial vs. all residual plot. It is seen that there appear to be no large variations at first, but after 6000 years and oscillation starts up and grows as a function of t^2 . This indicates that the oscillation is not real and is only due to noise.

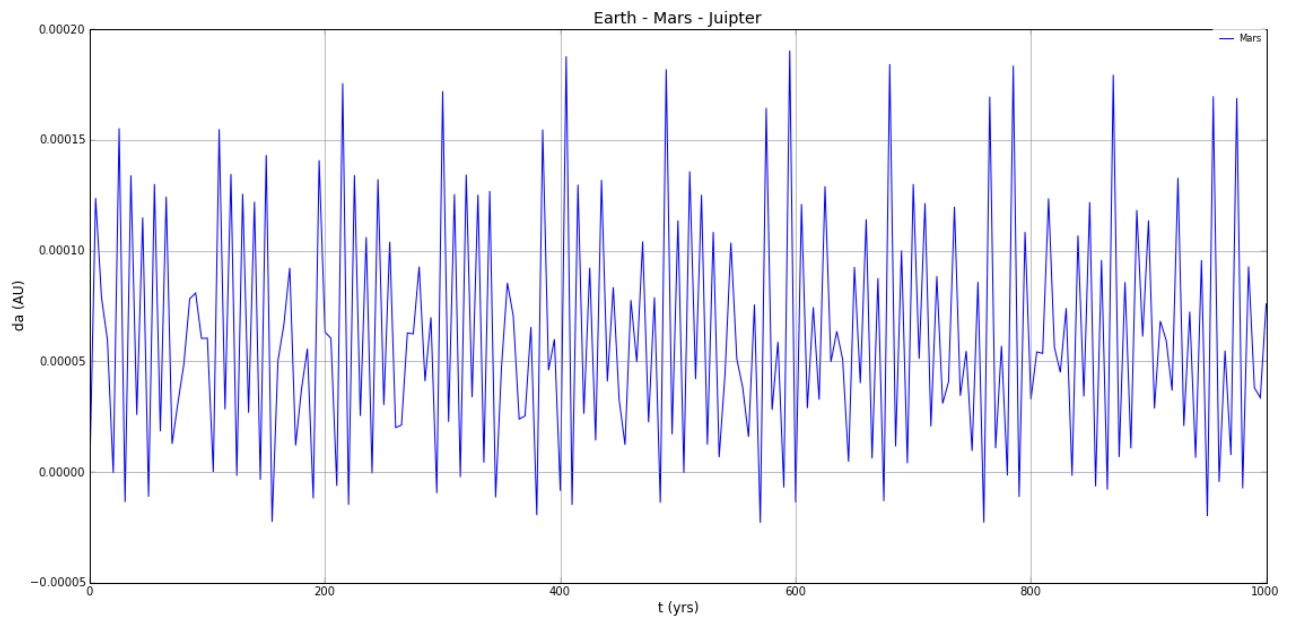


Figure 4: Plotted are the residuals in Mars' semi-major axis from an integration of only Mars vs. one of Earth, Mars and Jupiter. This was a baseline test, to qualitatively determine the perturbative effects of planets on each other.

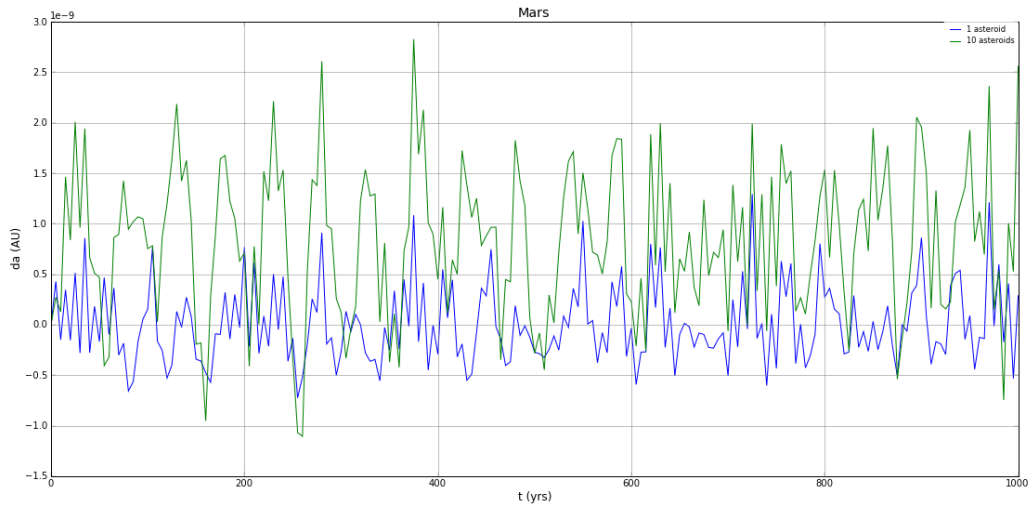


Figure 5: Plotted are the residuals in Mars' semi-major axis from an integration with Earth, Mars, and Jupiter, and compared to the same integration with 1 or 10 asteroids. This shows the degree to which the gravitational perturbations increased with an increase in perturbing bodies.

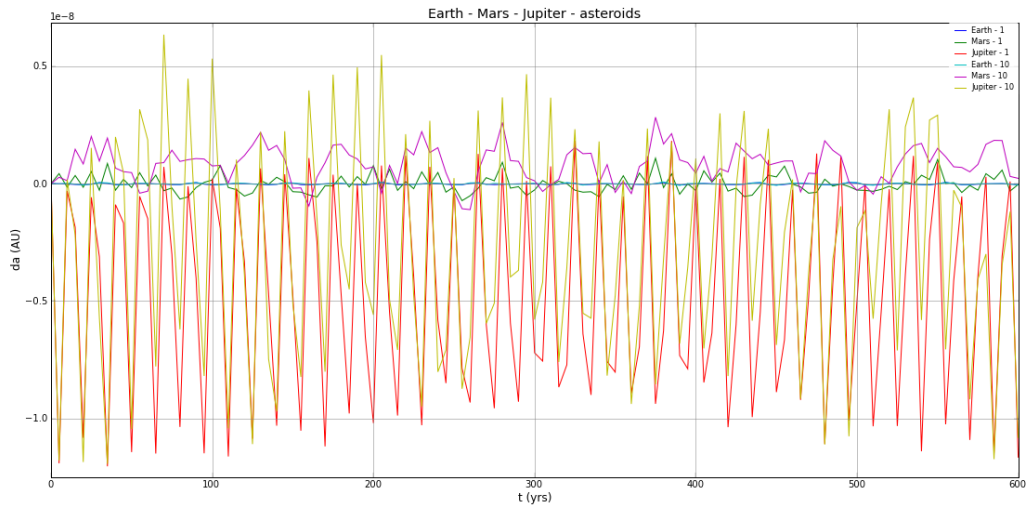


Figure 6: Plotted are the residuals in semi-major axis for Earth, Mars and Jupiter for integrations including either 1 asteroid or 10 asteroids. This shows the large differences between the perturbations on the three planets.

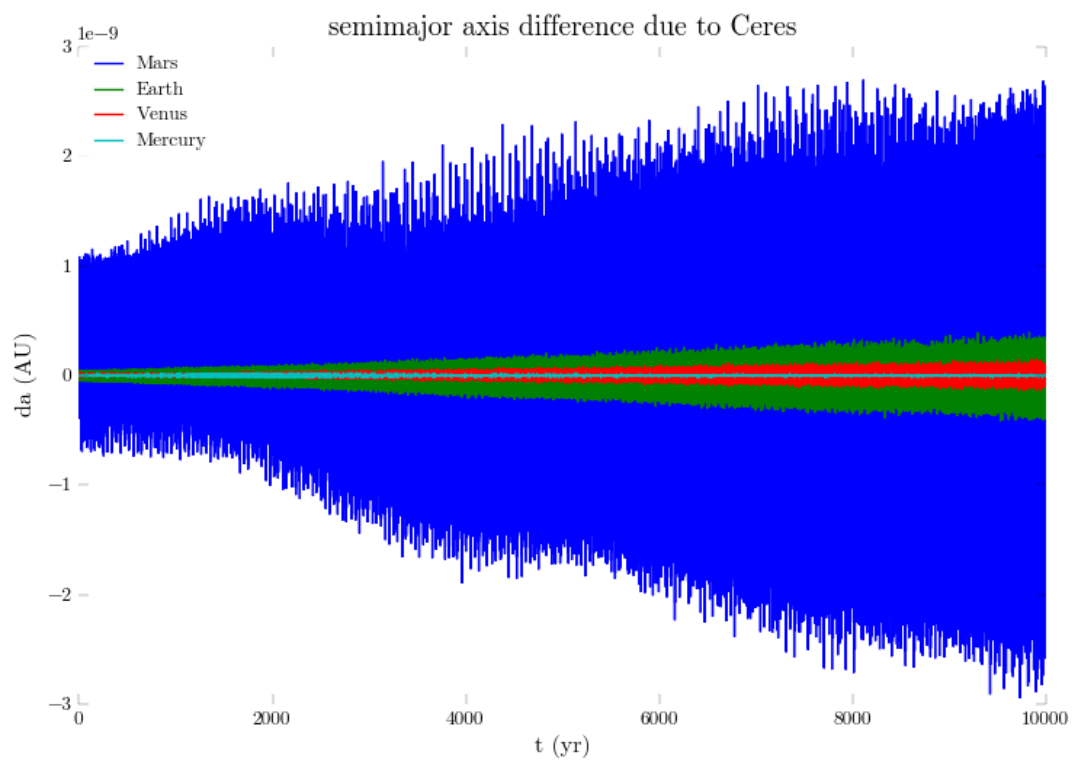


Figure 7: A residuals plot for a 10,000 year integration of the 8 planets and Ceres, the largest asteroid. This shows the relative effects that Ceres has on planetary motion, and that Mars is the most heavily affected among the inner solar system planets.

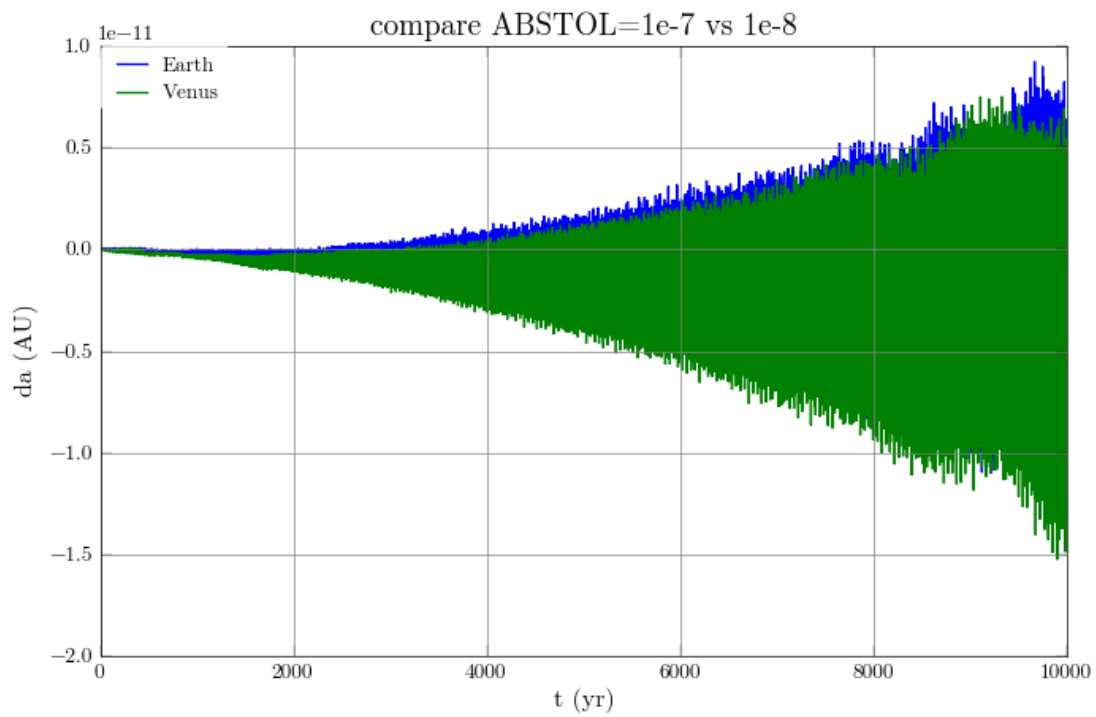


Figure 8: A plot of the residuals from two runs with different absolute tolerances. Compare this scale to that of figure 9 to find it is an order of magnitude smaller. This indicates that an error tolerance of 1×10^{-7} is sufficient.

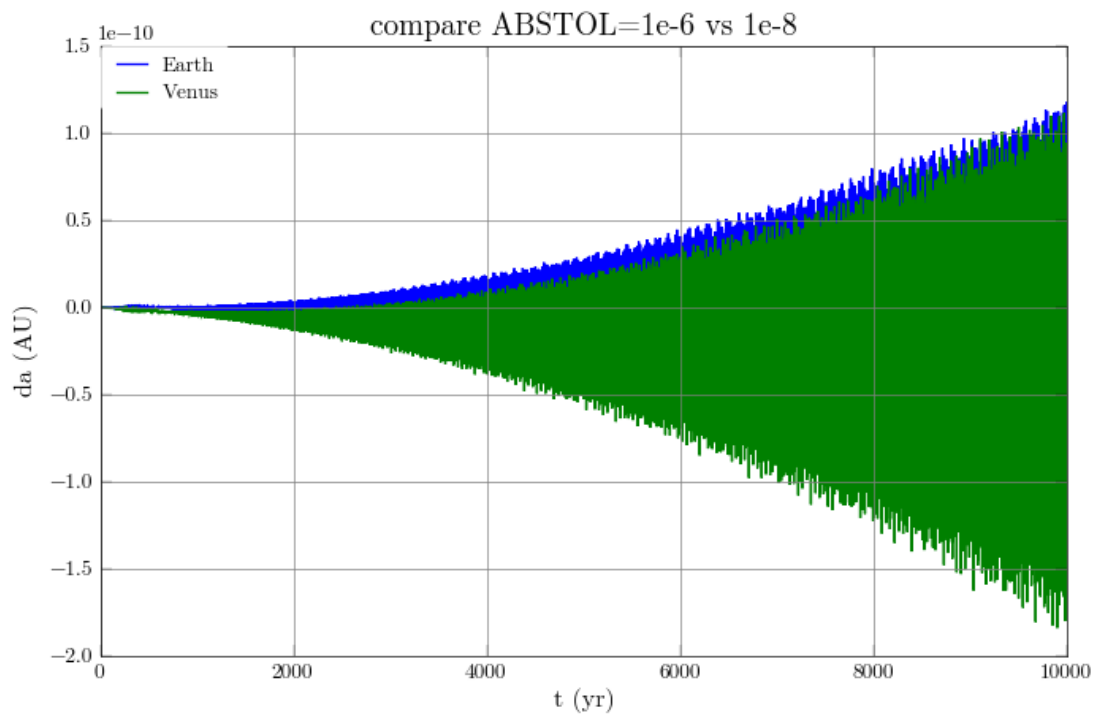


Figure 9: A plot of the residuals between two different levels of absolute tolerance. Compare to figure 8. This scale is an order of magnitude larger.

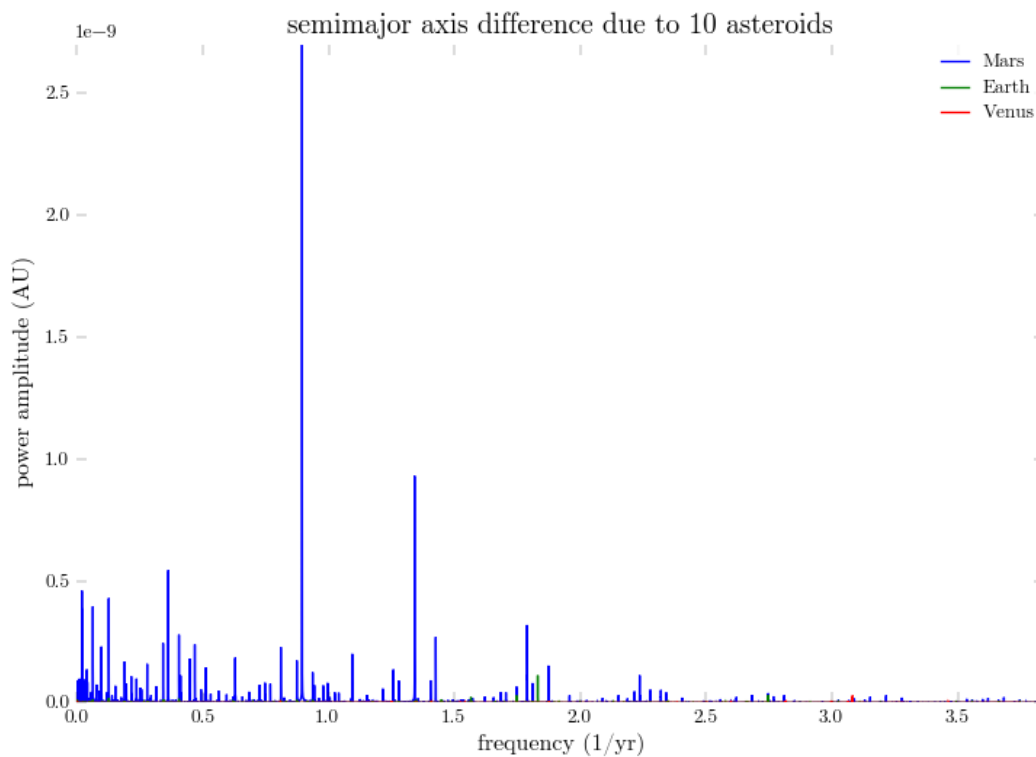


Figure 10: Plotted are the power spectra for Venus, Earth, and Mars from a 10,000 year integration with all 8 planets and 10 asteroids. It is clearly visible that the perturbations on Mars are the largest and that the frequency peak occurs at ~ 0.9 , which is once every 1.11 years. This means that Mars' semi-major axis is perturbed the most at a frequency ~ 0.9 , and that the perturbations on Earth and Venus are significantly smaller. Also observed are two large wings on either side of the Mars spike. These are either cause by numerical noise, or by chaos. The magnitude of these perturbations on Mars is on the order of 153 m.

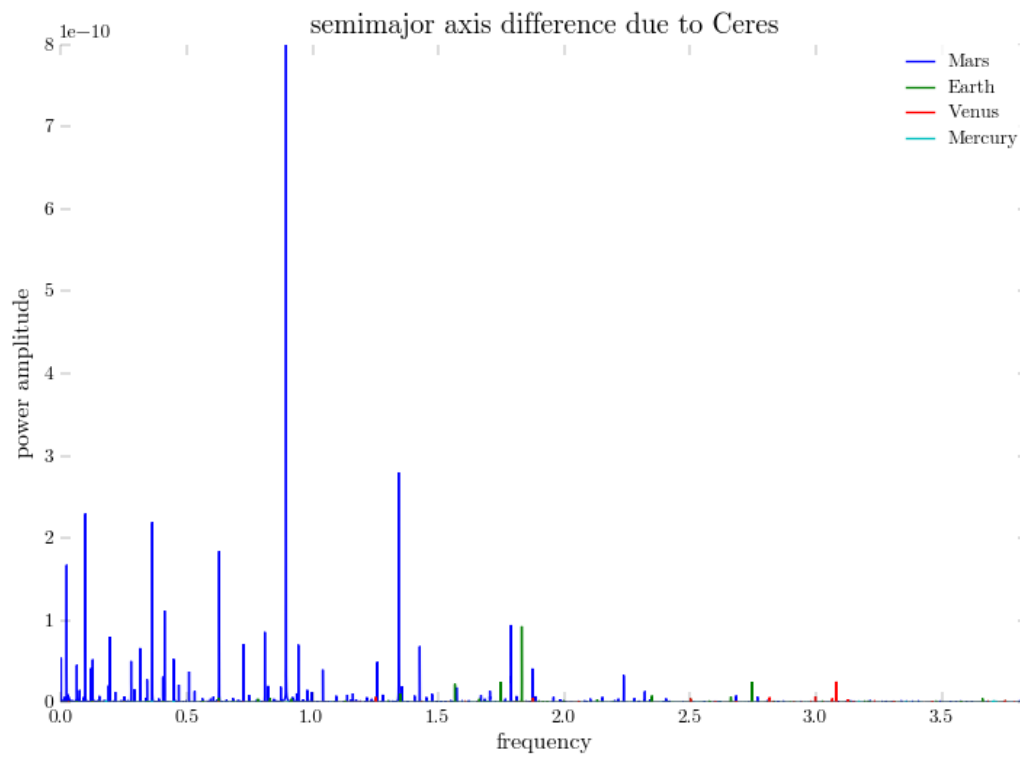


Figure 11: Plotted are the power spectra for a 10,000 year integration with all 8 planets and only Ceres, the largest asteroid in the asteroid belt. The power spectra here, as compared to those seen in figure 4, are not significantly different but do show the influence of multiple asteroids on planetary motion.